A Test of the Role of Longwave Radiative Transfer in a General Circulation Model

STEPHEN B. FELS[1] AND LEWIS D. KAPLAN

Department of the Geophysical Sciences, The University of Chicago, Chicago, Ill. 60637

(Manuscript received 19 June 1974, in revised form 29 October 1974)

ABSTRACT

The dynamical consequences of systematic changes in longwave radiative transfer computations have been investigated using the NCAR six-layer General Circulation Model. The experiments were run for a period of 40 days each: the "control" case with an emissivity computation, and the "test" case using a 19-spectral-interval calculation, in which the Curtis-Godson approximation is employed. The two calculations lead to substantially different cooling rates when applied to identical soundings, especially in the tropics.

Significant differences are observed in the thermal structure of the two cases, and in the mean meridional circulations. The total kinetic energy is somewhat higher in the test case, probably due to increased baroclinic activity in mid-latitudes.

1. Introduction

Although the best available methods of calculating infrared flux divergence usually give roughly the same average tropospheric cooling rates, the vertical gradients of the computed cooling differ by as much as a factor of 2 (see Rodgers and Walshaw, 1966). Since infrared flux divergence seems to be responsible for the bulk of the non-adiabatic temperature changes in the middle and upper troposphere (Washington, 1971), and since these differences appear to be systematic, it is likely that oversimplified schemes of introducing radiative effects into general circulation and numerical prediction models could result in systematic errors in the calculated production of available potential energy.

One of us (Kaplan, 1954, 1959, 1960) has, for some time, cited this probability of errors in space gradients of the cooling rates as a reason for performing accurate cooling rate calculations. The question is still controversial, however.

Washington (1971) has reported negative results on the effect of random radiation errors on global mean temperature in the NCAR six-layer model, but left open the question of the effect of systematic errors. It is this question that the present study addresses.

In order to test the effect of systematic radiation errors on model calculations of atmospheric structure and circulation, we have conducted a numerical experiment using the National Center for Atmospheric Research (NCAR) six-layer General Circulation Model (GCM), in which the same dynamical model is run with two different longwave radiation computations: the original one, and a considerably more complex, and (presumably) more accurate one. Each case was begun from precisely the same initial data. These data consisted of the values of the various dynamical fields which existed at the beginning of the 40th day of a previous GCM experiment conducted some years ago by Kasahara and Washington (1971). This earlier case had been spun up from a static, isothermal initial state, and had come close to equilibrium by the 40th day, when our experiment begins. This particular case was chosen because it was a no-mountain run, and the inclusion of mountains so significantly increases the complexity of the new radiation scheme that the number of model days available for the experiment would have been seriously reduced.

Both cases were run for 40 additional days to day 80. We shall refer to the run using the original NCAR longwave radiation calculation as the "control case," and that using the new calculations as the "test case."

The NCAR model has been described by Oliger *et al.* (1970), and, aside from a brief discussion of the two different radiation computations, we need only mention a few relevant characteristics of the model which are especially important in interpreting our results:

1) Sea surface temperatures are fixed at climatological values, and are constant in time.
2) Solar declination is that for "perpetual January."
3) The model incorporates both moist and dry convective adjustment routines (see Olgier *et al.*, 1970).
4) Cloudiness is computed rather than specified.

[1] Present affiliation: Geophysical Fluid Dynamics Laboratory/NOAA, Princeton University, Princeton, N. J. 08540.

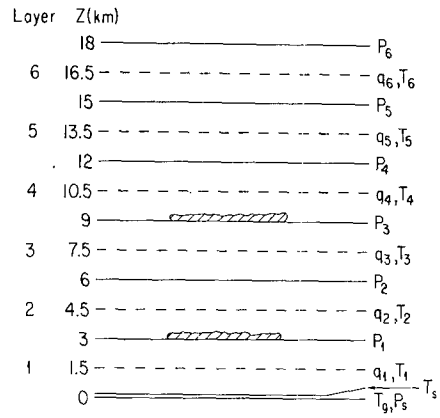

FIG. 1. Structure of NCAR 6-layer GCM. The two layers of clouds are shown as hatched regions.

It should be stated at the outset that the present study is intended as the first stage of a more ambitious project directed toward an understanding of the interaction of radiation and dynamics in the real atmosphere, but that this is not the problem that we have tackled here. Instead, we are merely asking whether radiation routines which give different values for the vertical and meridional radiative cooling rate gradients will yield significantly different model statistics. This question is one that must be answered, we felt, before constructing a more accurate and efficient radiation routine. We feel that we have, in the course of this study, not only provided an affirmative answer but also provided some insight into the nature of the radiation-dynamics interaction.

2. Radiation calculations

In Fig. 1 we show the layer structure of the NCAR model, and the position of the radiatively active clouds. These are treated as infinitely thin blackbodies just above 3 and 9 km.

The control case uses an extremely fast radiation calculation based on the Yamamoto chart (Sasamori, 1968, 1970). The temperature dependence of line intensities is neglected in the particular formulation used, and only water vapor and carbon dioxide absorption are included. Consequences of the fact that ozone is present in neither the control or the new radiation scheme will be discussed in Section 3.

TABLE 1. Random model parameters for the 6.3 μm band of H_2O. Symbols are those of Rodgers and Walshaw (1966, see their Table 5).

Interval (cm^{-1})	$k\delta^{-1}$ (g^{-1} cm^2)	$\pi\alpha_0\delta^{-1}$
1200–1350	15.0	0.075
1350–1450	256.6	0.120
1450–1550	1034.4	0.196
1550–1650	752.4	0.130
1650–1750	1175.8	0.167
1750–1850	381.9	0.128
1850–1950	69.8	0.084
1950–2050	11.8	0.080
2050–2200	11.8	0.080

The new scheme divides the infrared spectrum into 19 intervals and, within each one, calculates the net upward infrared flux by a finite-difference version of the transfer equation:

$$F^{\uparrow}_{\nu}(z_i)-F^{\downarrow}_{\nu}(z_i)=\left\{[B_\nu(\text{ground})-B_\nu(0)]\bar{\tau}_\nu(0,z_i)+B_\nu(\infty)\bar{\tau}_\nu(\infty,z_i)-\int_0^\infty \frac{\partial B_\nu}{\partial z'}\bar{\tau}_\nu(z',z_i)dz'\right\}\Delta\nu, \quad (1)$$

where $F^{\uparrow(\downarrow)}_{\nu}(z_i)$ is the upward (downward) infrared flux at level z_i in the frequency interval $(\nu-\Delta\nu/2,\ \nu+\Delta\nu/2)$, $B_\nu(z)$ the blackbody function at height z in the free atmosphere, $B_\nu(\text{ground})$ the blackbody function of the ground, and

$$\bar{\tau}_\nu(z,z')=\frac{1}{\Delta\nu}\int_{[\Delta\nu]}\tau_\nu'(z,z')d\nu',$$

the mean transmission function for interval $[\Delta\nu]$.

The important characteristics of the discretized version of Eq. (1) are the following:

1) Both schemes assume the atmosphere above 18 km to be isothermal, at a temperature equal to that linearly extrapolated from values at 13.5 and 15.5 km. Hence $B_\nu(\infty)=B_\nu(18\text{ km})$.

2) The lapse rate is assumed constant between the mid points of the layers.

3) Vertical quadratures are effected by Simpson's rule with ordinates calculated at 1.5 km intervals, save for a special "nearby layer" routine to be discussed below.

4) Eq. (1), which is only true for cloudless conditions, is modified in a straightforward manner to include clouds at 3 and 9 km, in precisely the same manner as is done in the control model, i.e., the clouds in these layers are treated as infinitely thin blackbodies.

5) Water vapor transmission functions are calculated using Godson's method with a Goody exponential model, as described by Rodgers and Walshaw (1966). Their model parameters are used for the rotational band, except that the sign of b for interval 10 in their Table 3 is corrected. For the H_2O 6.3 μm band the parameters have been calculated *ab initio* from the data of Benedict and Calfee (1967), and are given in Table 1. The temperature dependence of the line intensities which is ignored in the 6.3 μm band is taken into account in the rotational band by using a standard mid-latitude temperature sounding.[2] This significantly reduces the computation time.

[2] The overall contribution of the 6.3 μm band to heating rates is small due to its position well away from the blackbody peak. In addition, it is the strong lines which contribute importantly and these have weak temperature dependence. These two facts justify ignoring the temperature dependence of the line intensities in this band.

6) A constant, uniform mixing ratio for CO_2 is assumed, so that an extremely accurate off-line precalculation of transmission functions could be effected. These calculations, which assume a standard temperature sounding, were based on a line-by-line frequency integration furnished us by Dr. Virgil Kunde.

7) In those spectral intervals where absorption is strongest, the spectral variation of the transmission functions for small path lengths is too large to allow the use of Simpson's rule. For these "nearby layers," a fit of the form

$$\bar{\tau}(z_i,z')=\exp(-\alpha|z_i-z'|^{\frac{1}{2}}), \qquad (2)$$

using the exact value of $\bar{\tau}(z_i, z_{i+\frac{1}{2}})$ or $\bar{\tau}(z_i, z_{i-\frac{1}{2}})$, is made and analytically integrated. Tests show that the resultant cooling rate errors due to this particular error source are less than 0.02°C day^{-1} when compared with numerical quadratures using 256 points in the same interval.

The two schemes give rather different heating rates for a given temperature-humidity profile. This can be seen in Fig. 2 which shows zonally averaged heating rates yielded by each for latitudes 0, 20, 40, 60 and 80N at day 40½. (It should be made clear that, in this comparison, both radiation models use precisely the same temperature, humidity and cloudiness data, so that the figure is a true measure of the differences between the two computations. Fig. 3 shows the mean temperature cross section at day 40½.)

At both 80 and 60N, the new scheme cools the upper four layers by about 0.3°C day^{-1} more than the control, and in the second layer 0.4°C day^{-1} less. The net effect is to destabilize layer three relative to two, and to stabilize two relative to one.

In the tropics the new scheme cools the upper layer by over 1°C day^{-1} relative to the control, while the third layer is cooled less.

The reason for these differences is difficult to ascertain, since the schemes differ in many respects. The original computation does not include effects due to the temperature dependence of line intensity and the shift in the position of the blackbody peak with changing temperature. Empirically determined functional forms are used for the emissivities, and the vertical quadrature is less precise than that in the new scheme. We have estimated that the ignored temperature dependences can account for differences of as much as 0.3°C day^{-1} and, given the other factors mentioned above, the discrepancies are not unreasonable, except for the upper levels in the tropics. We find the heating produced by the control scheme in the tropical upper layer particularly difficult to understand, since O_3 is not included in either scheme.

The fact that the control does nonetheless give heating in these regions, and therefore to an exaggerated extent mimics the effect of O_3 in the real atmosphere, will have important consequences in the behavior of the dynamics.

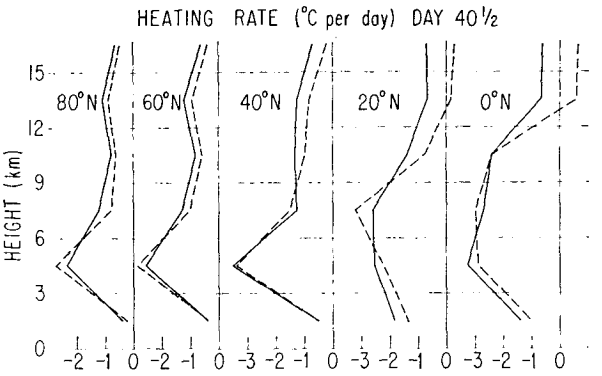

FIG. 2. Heating rates (°C day^{-1}) at day 40½ as calculated by test case (solid lines) and control case (dashed lines).

Given these differences, our attention now shifts to the main question under investigation: To what extent is the model atmosphere affected by them?

In discussing the question, we have found it useful to think in terms of two possible responses by the model atmosphere to changes in the radiation calculations.

We may imagine an idealized version of our experiment, in which we begin with an atmosphere which has equilibrated, driven by the original radiation calculation. Since this idealized model has no annual cycle, the total heating rate for any volume is presumably zero if averaged over a sufficiently long time. This heating consists of a "radiative" portion, and all the rest, which we shall call "dynamical."

The new radiation calculation, with altered heating rate, is now introduced, and the model integrated forward until equilibrium has again been reached, so that the total time-averaged heating is again zero. There are two extremes in the manner by which the

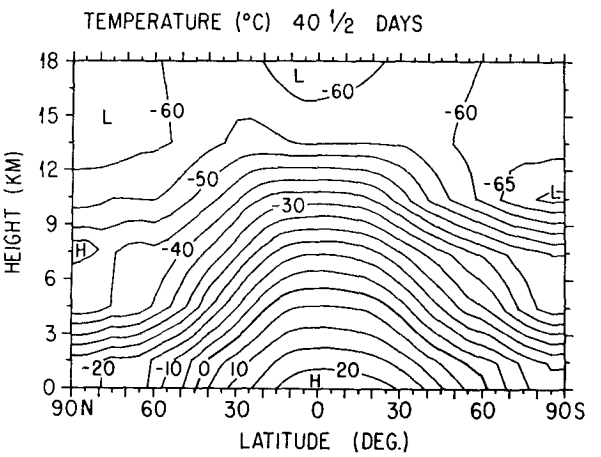

FIG. 3. Zonally averaged temperature at day 40½.

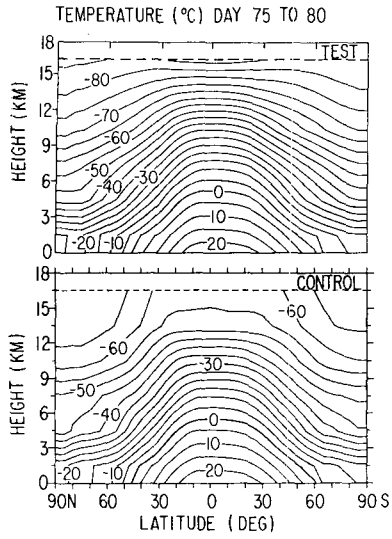

FIG. 4. Zonally averaged temperature for days 75–80.

new balance may be achieved:

1) "Radiative adjustment," in which the dynamical heating remains at its original value, but the temperature field is altered in such a way as to restore the radiative heating, calculated by the *new scheme* with the *new* temperature field, to that calculated by the *old* scheme with the *old* temperature field.

2) "Dynamic adjustment," in which the temperature and humidity fields remain constant, and therefore the radiative heating, which is altered immediately by the new radiation routine, stays at its altered value while the dynamics changes so as to make the total heating once again zero.

While we do not expect the results of the experiment to fit either of these descriptions exactly, they do provide a simple way of characterizing the changes which we shall discuss next.

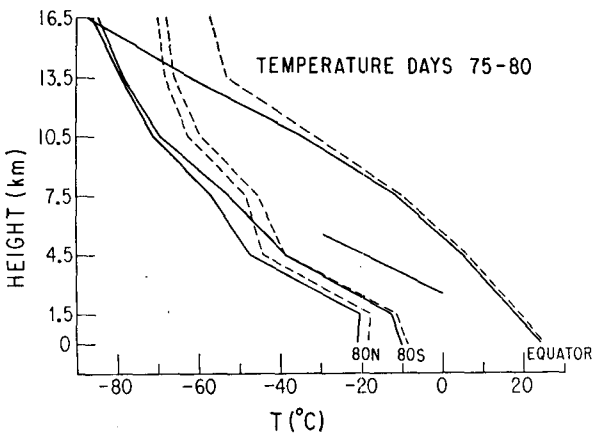

FIG. 5. Temperature vs height at 80S, 80N and 0 latitude for days 75–80. Test case: solid lines; control case: dashed lines.

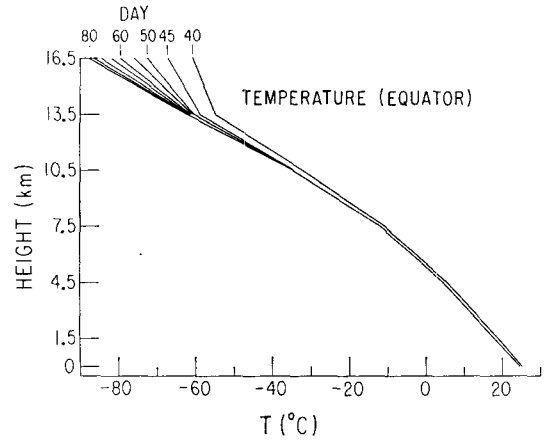

FIG. 6. Temperature vs height for test case, variation with time.

3. Thermal structure

It is not surprising that the most dramatic changes induced by the changed radiation computation are in the thermal structure of the atmosphere. In Fig. 4 we show zonal mean cross sections for the two cases, averaged from day 75 to 80. The same data are presented in graphical form for greater clarity in Fig. 5 for latitudes 0, 80S and 80N. At the equator, the new scheme has induced only slight cooling in the lower three levels, in spite of the substantially greater longwave cooling. This is to be expected from the fact that the sea surface temperature is fixed in the NCAR model; thus, the original radiation calculation produces sufficient cooling so that the lapse rate is controlled by convective adjustment. The increased cooling at these levels, therefore, merely induces more vigorous convection and leaves the temperature unchanged. It should not be thought, however, that this is without consequences—we shall return to this point subsequently.

In the upper equatorial atmosphere, the original radiation case does not cool sufficiently to allow complete convective control of the lapse rate, and the temperature changes drastically with time, especially in the uppermost layer (Fig. 6). By day 75–80, the

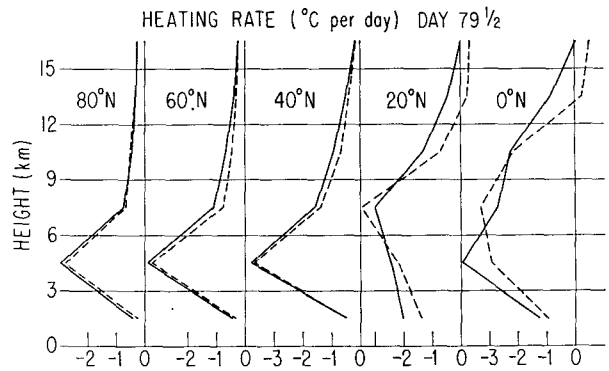

FIG. 7. Heating rates as in Fig. 2 for day 79½.

TABLE 2. Mixing ratio (g kg^{-1}), days 75–80.

Level (km)	80N		60N		40N		20N		Equator	
	Test	Control	Test	Control	Test	Control	Test	Control	Test	Control
1.5	0.56	0.77	1.64	1.49	4.55	4.68	10.43	11.39	14.49	14.96
4.5	0.11	0.12	0.23	0.24	0.98	1.02	1.40	2.21	5.76	5.89
7.5	0.019	0.067	0.050	0.080	0.20	0.21	0.93	1.35	1.79	2.98
10.5	0.004	0.016	0.009	0.021	0.025	0.063	0.061	0.110	0.25	0.42
13.5	0.002	0.012	0.003	0.015	0.006	0.026	0.005	0.029	0.019	0.041
16.5	0.001	0.004	0.001	0.005	0.001	0.007	0.000	0.011	0.000	0.012

equatorial temperature field has reached equilibrium, but now the convective region almost reaches the top of the model. There is no longer a tropopause in equatorial regions. This suggests that the tropopause in the original case was controlled by radiation.

In the polar region convective adjustment plays a secondary role, and important changes have taken place in the temperature of the lower troposphere, which has fallen by about 8°C at 7.5 km. The overall pole-to-equator temperature gradient in the lower levels has increased by 7°C.

It is worth noticing that while the control experiment gives a strong poleward decrease in temperature in the top layer, the new radiation case has a temperature maximum in this layer at about 40N, and in general, a less drastic poleward gradient above 10.5 km.

As the longwave cooling rate depends on the temperature structure, it is important to examine how it changes as the experiment progresses. In Fig. 7 we have plotted the cooling rates at day 80 as was done in Fig. 2 for day 40. In Fig. 7, however, the two radiation schemes are no longer producing cooling rates based on the same temperature and humidity fields, as was the case in Fig. 2; instead, the test scheme uses the fields of the test case on day 80, and the control scheme those of the control case.

At latitudes 80, 60 and 40N, the cooling rates generated by the new scheme with the new thermal structure are remarkably close to those generated by the original scheme; in the tropics, however, there are important differences. At both 20N and the equator, in the lower five layers, the differences between the cooling rates in the two cases are at least as large at day 80 as at day 40. It is only at 16.5 km that the cooling rate discrepancies have been significantly reduced. This is, of course, due to the large temperature change at that level.

At least in the specific GCM we are using, the adjustment to equilibrium after the introduction of the new radiation computation is, in the polar regions and mid-latitides, close to that we have called "radiative" earlier. A change in the infrared calculations results in an altered temperature profile so as to bring the final longwave cooling rate back to the value it had before any changes were made. In the tropics, on the other hand, the adjustment is more nearly "dynamical," the changed infrared cooling rates being compensated for by non-radiative processes, primarily convection.

In the second layer (layer 2 of Fig. 1) the cooling rate at all latitudes on day 80 is greater than at day 40; the difference is about 0.6°C day^{-1} at the equator, 0.4°C day^{-1} in mid-latitude, and 0.8°C day^{-1} in the polar regions. This is due to several effects; somewhat surprisingly, changes in cloudiness is not one of these. Off-line computations show that heating rate changes due to this source are unsystematic. The largest of them, whose magnitude is 0.26°C day^{-1}, is in the wrong direction to explain the observed difference.

The lowered temperature in the upper troposphere results in an increase in the net upward infrared flux at the top of layer 2 (which, it will be recalled, carries infrared-active clouds). The net flux at the bottom of the layer has changed less, since the temperature of the ground and layer 1 have changed little, so that the flux divergence in the second layer is decreased. Calculations show that this can account for about 0.1°C day^{-1}.

A more significant mechanism depends on the fact that the upper layers of the model contain far less water vapor in the present calculation than those of the control case. This is seen clearly in Table 2, and is probably due to both the cooling of the upper layers and the increased convective precipitation as a result of the consequent detabilization. The decrease in water vapor

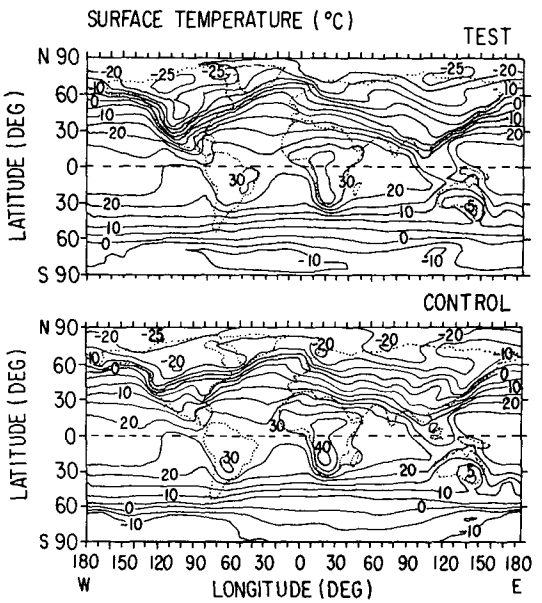

FIG. 8. Surface temperature (°C) at day 80.

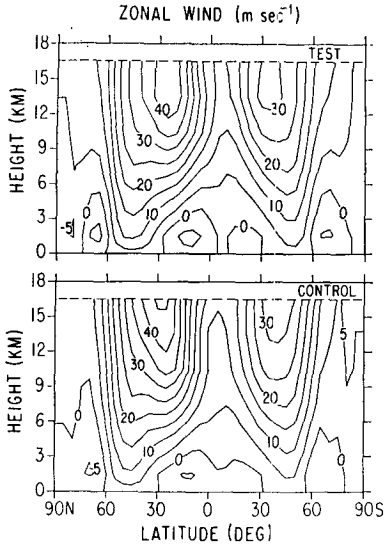

FIG. 9. Zonal wind component for days 75–80.

reduces the downward flux at the top of layer 2, resulting once again in increased cooling at this height. This can account for most of the observed increase.

Although zonally averaged surface temperatures show little change (on the order of 1°C at the equator, and 2°C near the poles), this is misleading since the sea surface temperature is fixed in the model. Fig. 8 shows the surface temperature for the two cases on day 80. There has been a drop of 6°C in the temperature maximum over southern Africa and the temperature minima in northern Canada.

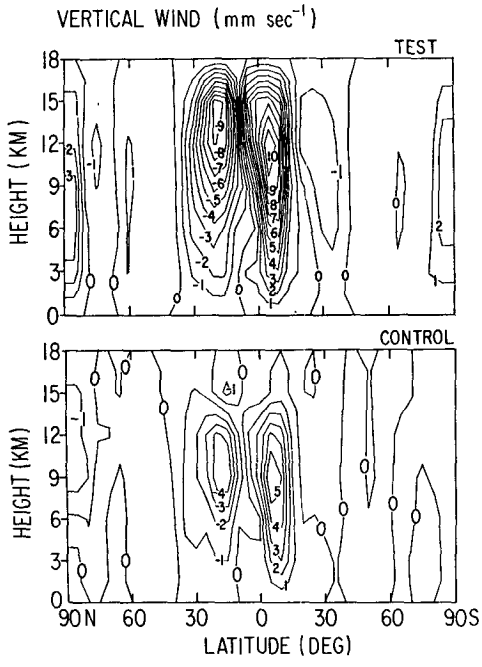

FIG. 10. Vertical wind component for days 75–80.

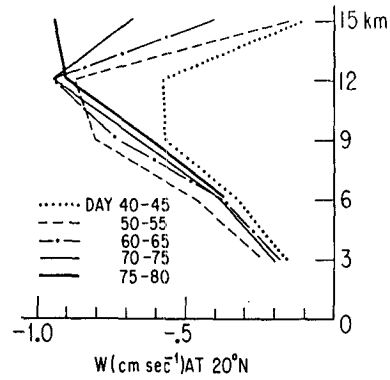

FIG. 11. Vertical wind component at 20N, variation with time.

It will be noticed from Fig. 4 that the equilibrium temperatures are too low at all latitudes in the test case upper layer—the tropopause has, in fact, everywhere disappeared. This is not surprising, since we have neglected both IR and solar heating by O_3 in order to be consistent with the control case. That the correction of our radiation routine by including the O_3 heating is likely to change the original upper-layer temperature configuration in the right direction can be seen by returning to Figs. 2 and 3, which show the meridional distribution of IR cooling (without ozone) and temperature, respectively, at day $40\frac{1}{2}$. The O_3 heating at middle latitudes, where the temperature distribution is a reasonable facsimile of the actual atmosphere, is of the order of the difference between the cooling rates of the two cases. On the other hand, it is too small to compensate for the upper layer cooling at low latitudes and will overcompensate at high latitudes. Thus the inclusion of O_3 in the radiation routine would move the temperature distribution in the upper layers toward the observed distribution. A quantitative discussion of these effects and their implications will be reported in a subsequent paper.

4. Zonally averaged velocities

While the changes in the temperature field are significant, our chief interest in this experiment is in the dynamical fields, as previously stated.

Fig. 9 shows the zonally averaged 5-day mean of U, the zonal component of the wind, between days 75 and 80 for the two cases. The primary difference is the lowering of the jet core from 16.5 to 13.5 km. Both maxima have moved equatorward by 5°, with no significant change in velocity. That we do get a truly closed jet can be inferred from the thermal wind relation, for at 13.5 km the new atmosphere has a much weaker pole-to-equator temperature gradient than does the control case, giving a vanishing horizontal temperature gradient at about 30N and 30S.

The changes in the meridional circulation are much more dramatic, especially in the tropics. Fig. 10 shows

TABLE 3. Diabatic heating rates (ergs cm^3 s^{-1}), averaged for days 75–80.*

Level (km)	Q_{DV} Control	Q_{DV} Test	Q_C Control	Q_C Test	Q_{LW} Control	Q_{LW} Test	Q_{SW} Control	Q_{SW} Test	Q_{Total} Control	Q_{Total} Test
					Latitude 5S					
0–3	7.5	10.8	50.0	58.6	−10.1	−11.1	4.2	3.9	51.6	62.1
3–6	0	0	10.4	13.5	−25.2	−32.0	4.8	5.7	−9.9	−12.9
6–9	0	0	10.1	13.9	−19.3	−17.4	4.8	4.3	−5.0	−0.9
9–12	0	−0.7	5.7	5.9	−11.7	−11.4	2.1	2.1	−4.0	−4.5
12–15	0.1	0.7	0.6	1.5	0.9	−2.9	0.5	0.8	2.0	−0.7
15–18	−0.1	0	0	9	1.0	−0.1	0.1	0.1	0.8	0.2
Sum	7.5	10.8	76.8	92.0	−64.4	−74.8	16.4	17.3	35.6	43.2
					Latitude 20N					
0–3	11.0	13.3	34.2	25.2	−16.8	−23.2	5.6	6.3	31.8	19.8
3–6	0	−0.1	1.9	3.6	−19.0	−20.2	2.0	1.5	−17.7	−18.0
6–9	0	0	2.2	2.2	−21.0	−19.0	3.2	3.3	−17.1	−14.0
9–12	0	−0.2	0.3	0.9	− 2.8	−5.4	0.6	0.6	4.6	6.4
12–15	0	−0.3	0	0.1	0.5	−1.3	0.2	0.4	0.1	−2.1
15–18	−0.1	0.5	0	0	0.6	0	0.1	0.1	0.4	0.8
Sum	10.8	13.3	38.7	32.1	−59.3	−69.0	11.8	12.1	−6.0	−20.0

* DV, vertical diffusion; C, condensation; LW, longwave; SW, shortwave.

the meridional structure of the zonal mean field of the vertical wind component W, averaged over days 75 to 80. Both the ascending and descending branches of the Hadley cell are almost doubled in strength relative to the control case.

The manner in which this difference establishes itself can be seen in Fig. 11, where we have plotted five day averages of W at 20N (the latitude of the descending maximum) for the periods 40–45, 50–55, 60–65, 70–75 and 75–80 days. The initial response is an increased circulation at all levels but most strongly at 12 km; by day 60, however, the lower part of the cell weakens somewhat, while the circulation continues to strengthen at 12 km and above. During the last period, the maximum has moved upward to 15 km, and reached a magnitude of 0.95 cm s^{-1}.

It is sometimes argued that circulation models are not sensitive to radiative changes in the tropics, since the thermal structure is so strongly controlled by the fixed sea-surface temperature and convective adjustment. The fact that we do produce short-term but significant changes in the field of vertical velocity shows that this is not completely true.

The increased depth and vigor of the Hadley cell are reflections of the drastically reduced static stability which our increased IR cooling has induced in the upper layers. In effect, we have removed the lid of stable air above 13.5 km which the control case possesses, and allowed the convective region to penetrate to the upper levels. In this context, it must be noted that the NCAR model has an artificial lid at 18 km; were this absent, the cell might be even higher.

It would be desirable to give a coherent discussion of the changed heat balance in the tropical regions, but our ability to do this is severely hampered by the fact that energy fluxes due to convective adjustment are not computed by the NCAR GCM diagnostic code. Nonetheless, we can examine the changes which have taken place in several of the most important energy transport processes: vertical diffusion, condensation, and long- and shortwave radiative heating. These results are presented in Table 3, which shows the various heat flux divergences averaged over days 75–80.

Looking first at 5S, it will be noticed that even though the total longwave cooling has increased, heating by condensation has increased in all layers but especially in the lowest layer so that, on balance, the 5S column is being heated more with the new radiation calculation.

The bulk of the effect, in fact, comes from the first layer. In the top half of the model where condensation is less important, there is increased cooling relative to

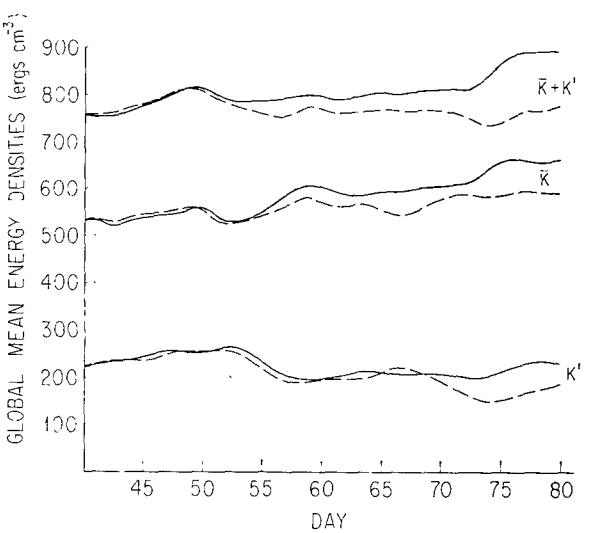

FIG. 12. Time variation of globally averaged mean zonal kinetic energy $\bar{K}$, mean eddy kinetic energy K', and total kinetic energy $\bar{K}+K'$ for test case (solid lines) and control case (dashed lines).

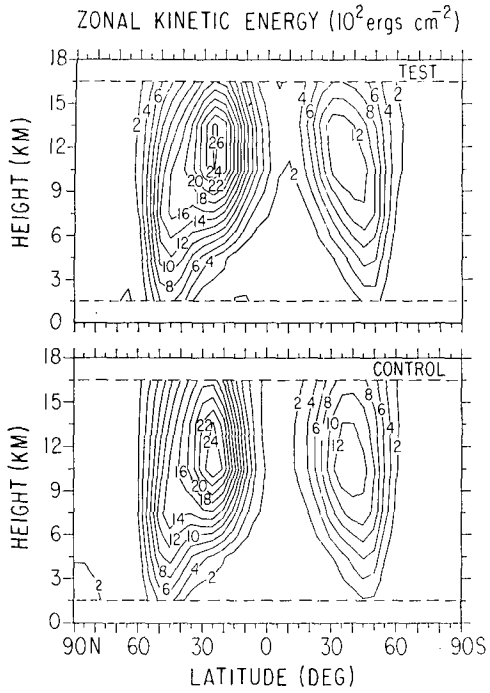

FIG. 13. Mean zonal kinetic energy for days 75–80.

the test case. The increased condensation heating in the lower layers is presumably due to the increase of moist convective adjustment as well as the increase of large-scale uplift.

The situation at 20N is somewhat different. In the lowest layer, the amount of condensation heating has decreased. This is reasonable in view of the lower humidity and increased downward vertical motion. In this layer, then, the differences in both radiation and condensation act in the same direction to give less heating.

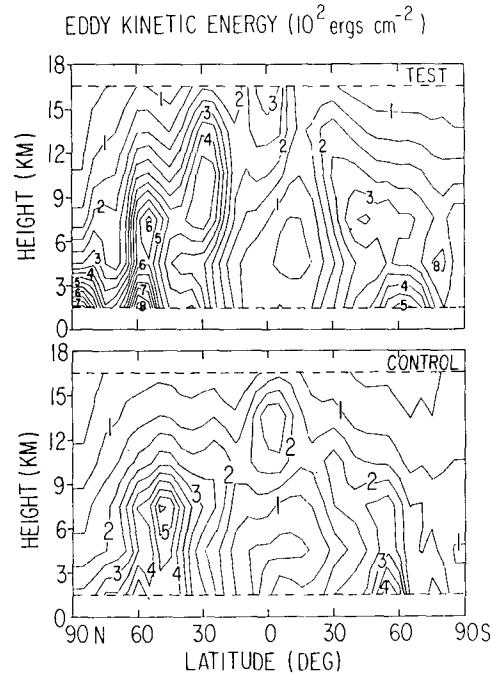

FIG. 14. Mean eddy kinetic energy for days 75–80.

At the 80th day, both cases are close to equilibrium, at least as measured by zonally averaged temperature and velocity fields, so that the increased net heating at 5S and cooling at 20N due to diabatic terms must be offset by dynamical processes (in which we include convective adjustment). It is clear that these changes in diabatic heating are consistent with the increased Hadley circulation.

5. Energy balances

In the 40 days of the experiment, there are significant changes in the energetics of the model. It is obvious that the total internal energy of the atmosphere must have decreased substantially, since the temperature in the upper layers has fallen. This is in fact true, the mean values (ergs cm^{-3}) being 9.62×10^5 on day 40 and 9.32×10^5 on day 80.

Far more interesting is the generation of kinetic energy K by the model. In Fig. 12 we have plotted the *global mean* values of $\bar{K}$, K' and $\bar{K}+K'$, where $\bar{K}$, the zonal mean kinetic energy, is defined as

$$\langle\bar{K}\rangle=\int_{-90^\circ}^{90^\circ}\cos\theta\int_0^{18\text{ km}}\tfrac{1}{2}\rho(\bar{u}^2+\bar{v}^2)dzd\theta\Big/\int_{-90^\circ}^{90^\circ}\cos\theta d\theta\int_0^{18\text{ km}}dz, \quad (3)$$

and K', the eddy kinetic energy, as

$$\langle K'\rangle=\int_{-90^\circ}^{90^\circ}\cos\theta\int_0^{18\text{ km}}\tfrac{1}{2}\rho(u'^2+v'^2)dzd\theta\Big/\int_{-90^\circ}^{90^\circ}\cos\theta d\theta\int_0^{18\text{ km}}dz. \quad (4)$$

Close examination of the graphs shows, particularly in the control case where equilibrium has been reached, that swings in $\bar{K}$ and K' are substantially opposite to each other—energy seems to slosh back and forth between the two. It is interesting that by day 60, the mean kinetic energy of the test case is noticeably greater than that of the control. The eddy energies stay close together until about day 68; at that time K' for the control drops, feeding energy in $\bar{K}$, so that the total remains substantially constant. K' for the test case, on the other hand, does not drop, and in fact rises slightly, so that the increase in $\bar{K}$ is uncompensated. The total effect is to produce a 15% relative increase in the total kinetic energy by day 80. The figure suggests that this is not a short-term fluctuation, but a secular tendency.

There have been no dramatic changes in the *distribution* of $\bar{K}$, as is seen from Fig. 13; while the maximum energy is almost the same in both cases, the jet is a bit more diffuse in the test case, leading to a higher total energy. The distribution of K' for the two cases averaged over days 75 to 80 is shown in Fig. 14. The two cases appear quite dissimilar. While some of this is due to statistical fluctuation, the differences around 55N are persistent.

As in the actual atmosphere, K' is large around this region, where the mid-latitude cyclone waves dominate. Since these represent the conversion of potential to eddy kinetic energy through baroclinically unstable waves, it is not far-fetched to suppose that the increase in K' might be explained by the intensified pole-to-equator temperature gradient. A measure of the strength of baroclinic instability is provided by the poleward eddy transport of heat, and in Fig. 15 we have plotted 5-day means of

$$\int_0^{18\text{ km}} \rho\overline{V'T'}dz,$$

the total poleward eddy heat transport, averaged between latitudes 50 and 60N and 50 and 60S. The large fluctuations in this quantity make it impossible to conclude that there has been any statistically significant change in the mean rate of poleward heat transport. From day 70 on, the eddy heat transport by the test case is larger in both the northern and southern baroclinic regions which agrees with the fact that at this time the control case K' drops below that of the test. Whether this result will persist for later times is not clear.

In Section 3 we pointed out that by day 80 the longwave radiative heating rates poleward of 30° are very nearly equal for the test and control cases. Fig. 16 shows the *total* diabatic heating as a function of latitude averaged over days 75–80. The only significant differences are again those in the tropics, due primarily to increased convective activity with its consequent release of latent heat, as discussed earlier. In this context, it is of interest to look at the total diabatic heating in the tropics and polar regions for the two cases. Table 4 shows the diabatic heating for the zones 85–50S, 45S–45N and 50–85N in the two cases during the last 5-day period, averaged over the respective zone; for example, the entry for zone 85–50S is defined as

$$\langle Q\rangle_{85S-50S}=\int_{-85°}^{-50°}\cos\theta\int_0^{18\text{ km}}\rho Q(\theta,z)dzd\theta\Big/\int_{-85°}^{-50°}\cos\theta d\theta\int_0^{18\text{ km}}\rho dz,$$

where Q is the total diabatic heating (°C day^{-1}). The difference in all zones are within the limits of statistical

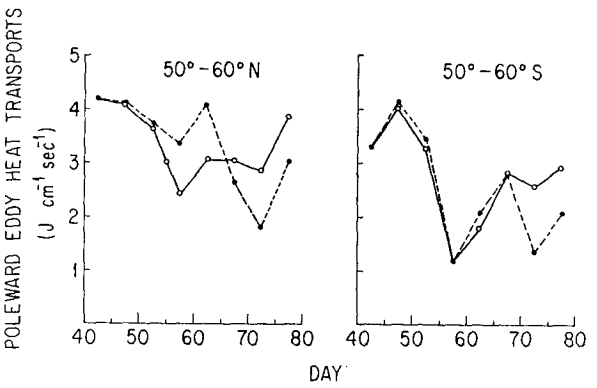

FIG. 15. Poleward eddy heat transport function ($\rho\overline{V'T'}$) as a function of time, averaged over 5-day periods. Test case: solid lines; control case: dashed lines.

fluctuation, indicating that the increased heating and cooling at 10S and 15N largely cancel.

6. Summary and discussion

In attempting to assess our results, it is important to realize that our concern in this paper has been with climatological changes induced by altered radiation. Under this rubric we include all of the various statistical properties of the atmosphere.

There can be no question that significant changes in the mean temperature field and meridional circulation have taken place in our experiment, as well as alterations in the global mean energy. The construction of an energy budget for the two cases is highly desirable but not possible with the limited statistics available.

The fact that the thermal structure in the tropics has been so drastically changed is especially interesting,

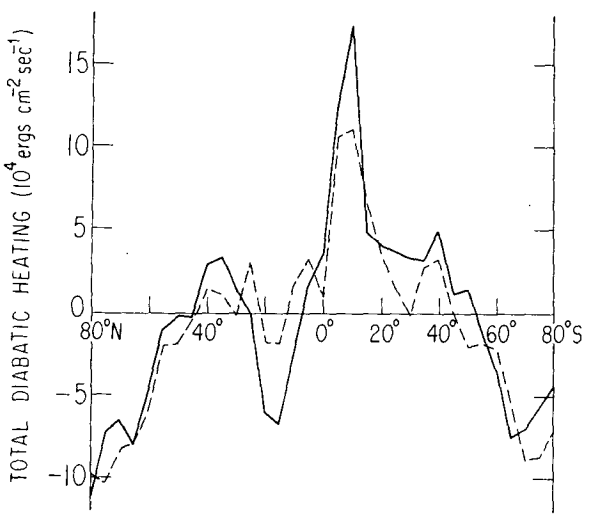

FIG. 16. Total diabatic heating (longwave+shortwave+condensation+diffusion) vs latitude, averaged for days 75–80. Test case: solid line; control case: dashed line.

TABLE 4. Mean total diabatic heating rates (°C day^{-1}), averaged over days 75–80 for polar and equatorial zones (see text).

Zone	Control	Test
85S–50S	−0.344	−0.261
45S–45N	0.216	0.240
50N–85N	−0.447	−0.384
85S–85N	−0.056	−0.093

for it raises the question of whether there is a critical cooling rate in the upper layers which leads to complete convective control of the thermal structure. Further investigation along these lines is under way with a more realistic radiation module including ozone heating.

The large changes in the Hadley cell which are produced also indicate the sensitivity of the tropical dynamics to altered radiative cooling. In this connection, it must be emphasized that the mean vertical velocity has changed significantly even in layers where the temperature structure is unaltered. This is an example of "dynamical adjustment," and serves to emphasize that merely because the thermal field is unaltered does not mean that other important changes may not have taken place.

Convective adjustment constrains the thermal structure less in the mid-latitude and polar regions, and here the adjustment is primarily "radiative"; there has been a significant temperature drop at all levels. The overall effect has been to *increase* the pole-to-equator temperature gradient. This may be responsible for the increased total kinetic energy we observe in the model atmosphere.

We have not as yet discussed an extremely important point which is the question of whether alterations in other portions of the model, such as convective adjustment, cloud prediction schemes, eddy mixing, etc., might not lead to much larger changes than those which we have observed in this experiment due to radiation. A separate but related problem is that even if the radiative transfer calculation is accurate, the humidity and cloud fields predicted by the model may have important errors which bias the resultant cooling rates.

Both are complicated questions. It seems likely that it is possible to preserve the accuracy of our radiation routine while significantly reducing the computation time it requires; this will be dealt with in future papers. If this is true, there is no reason not to use accurate calculation schemes, even though there remain other sources of systematic error in the GCM. The problem of the accuracy of the input to the radiation calculation is somewhat different. Our results suggest that it is primarily altered average static stability which is important, so that non-systematic errors in the water vapor and cloud fields may not be as significant as bias in the calculational algorithm. Systematic errors are more vexing. We have seen that there is an intimate coupling between radiation, dynamics and moisture content in the model atmosphere. It would be interesting, for example, to perform a companion experiment to the one we have described to assess the changes induced by an altered hydrological cycle.

It should be noted, finally, that the changes in the thermal structure and the meridional circulation in the tropics have already become appreciable during the first few days. Whether such short-term radiatively induced changes also take place at high latitudes, where the circulation is controlled more by the earth's rotation, will require a detailed diagnosis beyond the scope of the present paper and perhaps even of a single comparison of two cases. The question is of considerable meteorological importance, however, and is being investigated.

Acknowledgments. It is a pleasure to thank several people whose advice and assistance were essential to the completion of this project. Dr. Takashi Sasamori provided much useful information about both the overall design and the details of the radiation module used in the control run. Dr. Warren Washington gave us valuable advice both in the planning of the experiment and the analysis of the results. Gloria Williamson assisted with the insertion of the new radiation scheme into the NCAR GCM, and with the actual running of the experiments. Dr. Virgil Kunde furnished us with detailed CO_2 transmission functions which greatly simplified the construction of our radiation module. Finally, Man-li Wu provided invaluable help in the writing of the new radiation program, and performed extremely useful off-line computations which greatly aided us in interpreting our results.

This research was supported by Grant GA-32934 from the National Science Foundation and by the NCAR Advanced Study Program. The large amount of computation time needed as well as the use of the NCAR GCM program was furnished by the National Center for Atmospheric Research, which is sponsored by the National Science Foundation. This support is gratefully acknowledged.

REFERENCES

Benedict, William S., and Robert F. Calfee, 1967: Line parameters for the 1.9 and 6.3 micron water vapor bands. ESSA Prof. Paper 2, 204 pp. For sale by Superintendent of Documents, U. S. Govt. Printing Office.

Kaplan, Lewis D., 1954: The infrared spectrum of the lower stratosphere and its importance in the heat balance. *Sci. Proc. Intern. Assoc. Meteor.*, Tenth General Assembly, Rome, 583–591.

——, 1959: A method for the calculation of infrared flux for use in numerical models of atmospheric motion. *The Atmosphere and the Sea in Motion*, B. Bolin, Ed., Rockefeller Institute Press and Oxford University Press, 170–177.

——, 1960: Problems involved in introducing long-wave radiative effects into mathematical models. *Dynamics of Climate*, R. L. Pfeffer, Ed., Pergamon Press, 103–107.

Kasahara, Akira, and Warren M. Washington, 1971: General

circulation experiments with a six-layer NCAR model, including orography, cloudiness and surface temperature calculations. *J. Atmos. Sci.*, **28**, 657–701.

Oliger, Joseph E., Robert E. Wellck, Akira Kasahara and Warren M. Washington, 1970: Description of NCAR global circulation model. NCAR TN-56, National Center for Atmospheric Research, 94 pp.

Rodgers, C. D., and C. D. Walshaw, 1966: The computation of infra-red cooling rate in planetary atmospheres. *Quart. J. Roy. Meteor. Soc.*, **92**, 67–92.

Sasamori, Takashi, 1968: The radiative cooling calculation for application to general circulation experiments. *J. Appl. Meteor.*, **7**, 721–729.

——, 1970: Simplification of radiative cooling calculation for application to atmospheric dynamics. *Proc. WMO/IUGG Symp. Radiation Including Satellite Techniques*, WMO Tech. Note No. 104, World Meteorological Organization, Geneva, 479–488.

Washington, Warren M., 1971: On the role of radiation in dynamical climate simulation and numerical weather prediction. *Proc. Miami Workshop on Remote Sensing*, Environ. Res. Labs., NOAA, Boulder, Colo., 39–67.